Korean J. Chem. Eng., 36(7), 1184-1192 (2019)
DOI: 10.1007/s11814-019-0288-9

pISSN: 0256-1115
eISSN: 1975-7220

Screening of the antioxidant properties of olive (*Olea europaea*) leaf extract by titanium based reduced graphene oxide electrode

Sibel Yazar*, Ebru Kurtulbaş, Sinem Ortaboy*,†, Gülten Atun*, and Selin Şahin**,†**

*Istanbul University-Cerrahpaşa, Engineering Faculty, Department of Chemistry, 34320 Avcilar, Istanbul, Turkey
**Istanbul University-Cerrahpaşa, Engineering Faculty, Department of Chemical Engineering, 34320 Avcilar, Istanbul, Turkey
(*Received 1 March 2019 • accepted 27 April 2019*)

Abstract−Olive leaves were extracted with homogenizer-assisted extraction (HAE). Box-Behnken (BBN) design was employed through response surface approach (RSA) to achieve the optimum conditions. Bioactivity of the extract was assessed by its oleuropein, total biophenol (TBC) and total flavonoid (TFC) content along with its antioxidant activity determined by DPPH and CUPRAC assays. A new nanocomposite was developed using reduced graphene oxide (rGO) modified with TiOx (Ti-rGO) for trace amount determination of oleuropein in olive leaf extract. Structural characterization of the electrode was clarified using atomic force microscopy (AFM) and diffuse reflectance infrared Fourier transform spectroscopy (DRIFT) techniques. Cyclic voltammetry (CV) and square wave voltammetry (SWV) techniques were performed to investigate electrochemical behavior of oleuropein using three electrode configurations. Results of CV and SWV showed that quasi-reversible reaction occurred on electrode/electrolyte interface and a linear concentration range of 5-30 nM was obtained with a detection limit of 0.57 nM for oleuropein.

Keywords: *Olea europaea*, Food Analysis, Cyclic Voltammetry, Square Wave Voltammetry, Optimization

INTRODUCTION

Food waste production covers the whole food life cycle from agricultural to industrial production and processing, to retail and domestic consumption. In developed countries, 42% of food waste occurs in domestic consumption, while 39% of it is in the food manufacturing industry, 14% in the food services sector and 5% in the retail and distribution sectors [1]. Nowadays, industrial ecology concepts have been evaluated as a leading principle for eco-innovation that targets the *zero waste economy* where waste is used as raw material for new products and applications. Wastes in large quantities generated by food industries cause serious problems both economically and environmentally as well as a great loss of high-added value compounds. Moreover, most of these residues have reusable potential in other production systems.

The wastes of fruit and vegetable processes are the most worked resources for various types of antioxidants. The olive (*Olea europaea*) tree is one of the most important fruit trees of the Mediterranean countries, covering 8 million hectares, corresponding to about 98% of the world crop. This output demonstrates the economic and social importance of this crop [2]. Olive leaves, which are by-products of this crop, also represent 10% of the total weight of the harvested olives. This residue remains as an agricultural waste if not assessed [3]. Since olive leaf is a rich source of bioactive substances that have been proven many times in health effects, a wide variety of studies have been carried out in this regard [4]. However, the number of studies on olive leaf extract regarding the evaluation of antioxidant properties measured by electroanalytical techniques is quite inadequate. In particular, voltammetry provides fast, simple, inexpensive, accurate and precise analysis towards quantitative determination of electroactive species. Besides, this technique does not require complicated and time-consuming pretreatment processes [29]. Mohamadi et al. used DNA biosensor to measure the most prominent biophenol of olive leaf extract electrochemically [30]. Cittan et al. determined oleuropein by means of square wave voltammetric method [31]. Gomez et al. studied the pencil graphite electrodes to improve the electrochemical detection of oleuropein using the natural deep eutectic solvents and graphene oxide [32].

Carbonaceous materials have drawn tremendous attention in various applications due to their unique physical and chemical properties. Among them, the graphene family offers the most promising materials for the next generation smart devices, electrochemical sensors, biosensors, energy storage and conversion systems. Not only do they have excellent electronic, optical, physicochemical and biocompatible properties, but also they are the thinnest, stiffest and strongest material in the world [33-39]. Various synthesis methods are available to produce GO such as chemical vapor deposition (CVD) [12], extended Hummer's method [41], mechanical exfoliation [42] epitaxial growth [43] and electrochemical exfoliation [44]. The synthesis of GO via Hummer's method is a very cheap, rapid and effective process using graphite as the starting material [41].

Graphene oxide (GO) is composed of oxygenated graphene sheets containing oxygen functional groups such as carboxyl and hydroxyls on the edges and surfaces of the layers. This unique structure enables one to obtain large surface area and easy accessibility for

†To whom correspondence should be addressed.
E-mail: ortaboy@istanbul.edu.tr, selins@istanbul.edu.tr

different substances in molecular level [45]. This feature is important for the sensing field due to providing in the interaction of analytes with all carbon atoms in the structure. It is well known that reduction of GO to rGO increases the electrical conductivity and mobility of charge carriers [37], since structural defects and residual oxygenated group allow fast heterogeneous electron transfer, which is important to develop high sensitive electrochemical sensors and biosensors [43-46].

In this study, olive leaves were extracted with homogenizer-assisted extraction (HAE). Box-Behnken (BBN) design was employed through response surface approach (RSA) in order to comprehend the effects of parameters together with their interactions, where conventional optimizations methods do not consider during the change one parameter at a time [7]. Design of experimental study, optimization and modelling of the experimental data has been performed by the concerned RSA.

For further understanding, cyclic voltammetry (CV) and square wave voltammetry (SWV) techniques were performed to investigate the electrochemical behavior of olive leaf extracts. In this regard, a GO based electrochemical sensor has been developed for sensitive determination of trace amount of oleuropein, which is the main component of the olive leaf extract [37]. The sensor electrode was prepared by the modification of glassy carbon electrode using the nanocomposite containing titanium (IV) isopropoxide and reduced graphene oxide (Ti-rGO@GC).

MATERIALS AND METHODS

1. Plant and Chemical Materials

Olive leaf samples were supplied from Özgün Olive, Olive Oil Co. Olive leaf samples were provided from Agean (Ayvalık, Turkey) at harvesting time for oil production. The dried leaves were ground (Moulinex Super Blender Grinder, LM209041) and screened through a 22-mesh sieve.

Ethanol (>99.5%), methanol (>99.8%), isopropanol (>99.7%), H_2O_2 (30%), H_2SO_4 (>95%) and $NaNO_3$ were from Merck (Darmstadt, Germany), while sodium carbonate, Folin-Ciocalteu, 2,2-diphenyl-1-picrylhydrazyl (DPPH•), 2,9-dimethyl-1,10-phenanthroline (neocuproine), 6-hydroxy-2,5,7,8-tetramethylchroman-2-carboxylic acid (trolox), gallic acid, oleuropein, Ti(IV) isopropoxide (TTIP, ≥99.7%), graphite powder (~100 μm), potassium permanganate ($KMnO_4$, ≥99.7%), HCl (≥37%), formic acid (98-100%) and acetonitrile (≥99.9%) were from Sigma-Aldrich (St. Louis, MO, USA). Deionized water (DI) was provided by a Millipore Direct-Q3 system (≥18 M Ω cm)

Table 1. Process parameters for the HAE of olive leaves with their units, symbols and levels

Process parameters	Units	Symbol	Levels		
Time	sec	X_1	30	60	90
Speed	rpm	X_2	5000	7500	10000
EtOH concentration	%, v/v	X_3	20	50	80

2. Homogenizer-assisted Extraction

Leaf samples were extracted three times by ethanol-water solution (v/v) of different concentration by means of IKA T25 (ULTRA-TURRAX) brand homogenizer. The homogenizing conditions were adjusted to several conditions (Table 1). Before analysis, the extracts were filtered through a syringe filter (0.45 μm), and kept in dark at −20 °C.

3. Spectrophotometric Analyzes

Total biophenol (TBC) determination of the extracts was carried out spectrophotometrically (PG Instruments, T60/Leicestershire, England), depending on the Folin-Ciocalteu method [8], while total flavonoid content (TFC) was assessed by a modified procedure at 510 nm [9]. Free radical scavenging activity against DPPH radical was also used by following the report of Yu et al. [10] with some modifications [11]. Moreover, cupric ion reducing antioxidant capacity (CUPRAC) assay was applied to measure the antioxidant activity of the extract [12].

4. Chromatographic Analysis

Oleuropein concentration (OC) was measured by high-performance liquid chromatography (HPLC). Conditions of HPLC are given in Table 2.

5. Box-Behnken Design

As an experimental design method, RSA has been used for optimization of the HAE conditions and modelling the experimental data as well as design of experiments for the olive leaf extraction. In the relevant system, Box-Behnken (BBN) design was applied with the parameters as seen in Table 1. Time for the olive leaf extraction (X_1), speed of the homogenizer (X_2) and ethanol (EtOH) concentration of the solvent system (X_3) were selected as independent process parameters, whereas OC was the dependent parameter (Y). Design-Expert software (version 11) was exploited in order to able to apply the BBN to the relevant HAE system.

In this methodology, a second-order polynomial model is pro-

Table 2. Analyzing conditions of oleuropein content along with the gradient program applied

HPLC conditions	Program		
Model: Agilent 1260 (Agilent, Waldbronn, USA)	Time (min)	A (%)	B (%)
Colon: Agilent Eclipse Plus C18 RRHD 18 (3 mm×5 mm; 1.8 μm)	0.0	100	0
Mobile phase: A=Water+% 0.1 formic acid (v/v)	0.5	100	0
B=Acetonitrile+% 0.1 formic acid (v/v)	7.0	60	40
Detection wavelength: 276 nm	7.1	0	100
Flow rate: 1 mL/min	8.6	0	100
Column temperature: 40 °C	8.7	100	0
Injection volume: 20 μL	10	100	0

posed to form an empirical equation as presented with Eq. (1):

$$Y = \beta_0 + \sum_{i=1}^{k} \beta_i x_i + \sum_{i=1}^{k} \beta_{ii} x_i^2 + \sum_{i=1}^{k-1} \sum_{j=i+1}^{k} \beta_{ij} x_i x_j + \varepsilon \quad (1)$$

where β_0 is the constant coefficient, and β_i, β_{ii} and β_{ij} are the linear, quadratic, and second order interaction coefficients (i and j=3), respectively.

6. Statistical Analysis

ANOVA test (analysis of variance test) was used to determine the adequacy of the proposed second-order models as well as the effect of process parameters on the response. Sufficiency of the developed model was assessed by indicators such as correlation coefficient (R^2), adjusted correlation coefficient (R^2_{adj}) and *lack of fit* value through ANOVA test formed by Design-Expert software. For validation of optimum adsorption conditions, the difference between the results of actual and estimated by the proposed model was defined by ERROR (%).

7. Electrochemistry

All electrochemical measurements were performed at room temperature on a Gamry Reference 600 potentiostat/galvanostat system with a typical three-electrode system. For this electrochemical cell, an Ag/AgCl electrode and a platinum plate were used as the reference and the counter electrodes, respectively. Glassy carbon electrode (GCE) modified with Ti-rGO nanocomposite was used as the working electrode. The surface of the GC electrode (3.0 mm in diameter) was polished with 0.1 and 0.05 μm alumina slurries using a polishing cloth to obtain a mirror finish, and then ultrasonicated in (deionized) DI water and ethanol, successively. EChem Analyst 5.38 software package was applied for plotting and graphing electrochemical data.

8. GO Synthesis

Graphene oxide (GO) was synthesized according to Hummer's method [58]. In a typical procedure, two grams of graphite powder and 2 g of $NaNO_3$ were taken in 50 mL of H_2SO_4 in a 1,000 mL rounded flask. The mixture was kept under in an ice water bath (0-5 °C) for 2 hours. Then, 6 g of potassium permanganate ($KMnO_4$) was added to the mixture very slowly under stirring condition for 2 days at 35 °C. Prepared solution was gradually diluted by using 100 mL of DI water, and the temperature of the solution was increased to 98 °C. Later, 10 mL of 30% H_2O_2 (w/w) aqueous solution was added until the color of the mixture turned to yellow. The mixture was centrifuged with 10% HCl, and washed several times with DI water for the purification. The resulting mixture was dried at the room temperature until the GO was obtained as a black powder.

9. Reduced Graphene Oxide (rGO) Synthesis

The reduced graphene oxide (rGO) was prepared using the GO and ascorbic acid, which is the reductant in the reaction [48]. GO (5 mg) was stirred in 50 mL of DI water, and kept in the ultrasonic bath for 30 min. 0.1 M ascorbic acid was mixed with GO suspension with the volume ratio of 1 : 1, and heated to 70 °C using hot plate. The colloidal solution was stirred until the color of the mixture changed from the brownish-yellow to black. As prepared cloudy solution was centrifuged at 5,000 rpm and rGO samples were washed with ethanol and DI water several times and dried at 120 °C in an oven.

10. Preparation of Ti-rGO@GCE Electrode

The sol-gel method was used to prepare Ti-rGO nanocomposite. 7 mL of TTIP was added to 15 mL isopropanol, and stirred for 10 minutes (Solution A). 2 mL of HCI was mixed with 10 mL isopropanol (solution B). Solution B was mixed very slowly with the solution A. The resulting solution was stirred for 30 min. rGO was dispersed by ultrasonic bath in DI water containing 0.05 M AA. Ti-rGO composite material was obtained as an orange-colored gel. 10 μL of Ti-rGO composite gel deposited onto the glassy carbon electrode (GCE) using simple drop casting method, and was kept under ambient condition for 6 hours.

11. Characterization of the Electrodes

The structural characterization of electrodes involved AFM (Nanomagnetics Instruments) operated in tapping mode using aluminum coated silicon probes at room temperature. Pure GCE and Ti-rGO@GCE surfaces were scanned with 5 μms^{-1} scanning rate and 256×256 pixels resolution to get a view of 5×5 mm^2 area. The statistical parameters were calculated using the AFM images applying the NMI Viewer 2.0.7 software package program. All experiments were performed at room temperature (25±2 °C).

DRIFT spectroscopy was carried out using Bruker Alpha-T DRIFT spectrometer equipped with a 528/D model diffuse reflection unit containing double sample holders (3 mm deep, 6 mm in diameter). The mass ratio of the samples and KBr were kept constant at 1.5% (w/w). All spectra were collected by averaging 100 scans at a resolution of 4 cm^{-1}. OPUS 6.5 software (Bruker Optics Inc.) was used for the data acquisition.

RESULTS AND DISCUSSION

1. Characterization of the Electrochemical Sensor

To evaluate the interfacial behavior of the electrode surface, it is indispensable to know some significant structural properties such as height profiles, surface distributions and the roughness parameters of the electroactive surface. In this regard, AFM technique was carried out to realize the morphological and nanostructural formation of as-prepared electrodes. This technique provides visualization of the deposited materials in nanometer resolution.

Morphological structure of the GCE and Ti-rGO@GCE characterized by AFM technique is shown in Fig. 1(a)-(d). To provide further information about the surface textures, the root mean square roughness parameters (SRMS) and average surface roughness parameters (Sa) were calculated using the AFM 3D images. It was revealed that both of the roughness parameters were higher for TiOx-RGO@GCE (SRMS=65.20 nm, Sa: 4.32 nm) than those of GCE (SRMS=53.48 nm, Sa: 2.47 nm) surface.

Fig. 1(a) shows the surface morphology of the bare GCE. As shown, electrode has a flat surface and is fairly uniform in shape, and due to the cleaning-polishing procedure, scratches on the surface are clearly visible. From the cross-section image, the depth profile changes between the 12-28 nm (Fig. 1(b)). For Ti-rGO@GCE, 3D AFM image is presented in Fig. 1(c). When compared to the bare GCE, it is obvious that Ti-rGO@GCE is fully covered by the Ti-rGO nanocomposite. A porous and spiky peak distribution is observed on the surface and the depth of the pores changes between in 120-380 nm (Fig. 1(d)). The average particle size of the nanocomposite covering the surface changes between 30-800 nm. The porous structure of the Ti-rGO enables high surface area, which

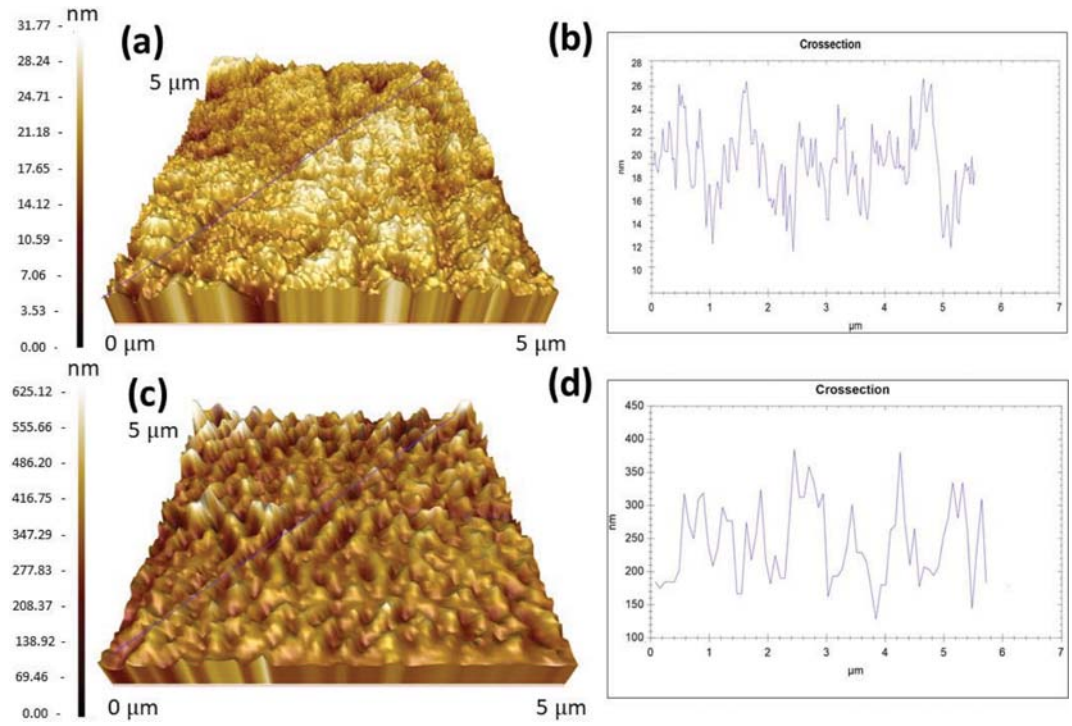

Fig. 1. 3D AFM images and depth profiles of the (a), (b) GCE and (c), (d) Ti-rGO@GCE electrodes, respectively.

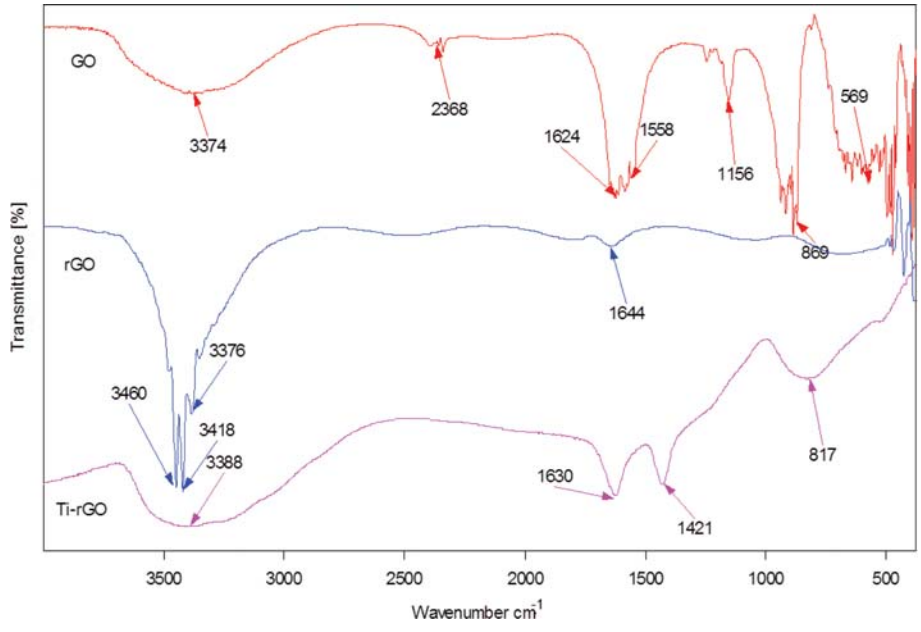

Fig. 2. The DRIFT spectra of GO, rGO and Ti-rGO samples.

is one of the most important factors to enhanced sensing ability of the electrochemical sensor.

DRIFT spectroscopy technique has some advantages, such as easy, fast and non-destructive sample preparation, high reproducibility, accuracy, and time-efficiency. This technique enables one to study a large variety of samples including films, powders, solids and liquids [49].

Fig. 2 shows the DRIFT spectra of the GO, rGO and Ti-rGO nanocomposite. GO sample shows a broad band at around 3,300 cm^{-1} indicating O-H stretching vibration caused by surface hydroxyl groups. When compared to the other spectra, it is clear that Ti-rGO has more O-H stretching vibration, originating from Ti-O-H groups. In case of rGO sample, sharp and prominent peaks are observed at about 3,460, 3,418, and 3,376 cm^{-1} indicating O-H stretching vibrations of ascorbic acid used in the reduction process of GO to obtain rGO samples [50]. For GO spectrum, the peak located at

2,368 cm^{-1} arises from the CO_2 in the air. The sharp peaks observed at 1,624, 1,558 cm^{-1} are attributed to the C=O and C=C ring stretching vibrations, respectively [23,24]. Typically, the peaks at 1,156, 1,260 and 869 cm^{-1} are linked to the C-O, C-O-C and C-C ring stretching vibrations due to the acid interaction of graphite indicating oxygen-containing functional groups on the GO surface [53]. All these prominent peaks disappear and the intensity of the peak at about 1,640 cm^{-1} decreases after the reduction process of GO suggesting the major part of the -COOH groups located on GO have been removed from the surface [54]. For Ti-rGO sample, the characteristic peaks at about 1,630 and 1,421 cm^{-1}, which are attributed to the C-C ring stretching and C=C stretching vibrations, dominate in the spectrum, indicating the existence of graphene domains in the structure. Compared to the rGO, the formation of a new broad band below the 1,000 cm^{-1} ensures the interaction of $Ti(OH)_x$ with rGO. The peak maximum observed at 817 cm^{-1} and the small peak at about 540 cm^{-1} are attributed to the Ti-O-Ti stretching and bending vibrations, respectively [53].

2. BBN Design and Adequacy of the Model

Table 3 summarizes the experimental study with 3 factors and 3 levels (lower, middle and upper) designed by RSA along with their coded values. The findings show the influence of extraction time (30, 60 and 90 sec), homogenizator speed (5,000, 7,500 and 10,000 rpm), and EtOH concentration of the solvent system (20, 50 and 80%, v/v) on the OC of the extracted olive leaf.

Second-order polynomial equation developed by RSA for the present extraction system is presented in Table 4. The high correlation coefficient (>0.94) verifies that 94% of the total variation in olive leaf extraction by HAE can be described by the relationship between the related independent parameters and the response (as given in Table 4). Only the remaining 6% of the total variation in Y cannot be explained by this equation derived by RSA.

Table 3. Effect of process parameters on HAE of olive leaves*

Run	X_1 (sec)	X_2 (rpm)	X_3 (%, v/v)	OC (mg/L)
1	60	5000	80	222.00±0.002
2	60	7500	50	236.00±0.001
3	90	5000	50	258.81±0.000
4	90	7500	80	272.36±0.003
5	60	7500	50	237.17±0.009
6	30	7500	20	159.85±0.000
7	30	5000	50	190.36±0.001
8	60	10000	80	285.11±0.001
9	60	7500	50	233.50±0.002
10	90	10000	50	320.65±0.002
11	60	7500	50	239.38±0.005
12	30	10000	50	189.36±0.001
13	60	7500	50	235.92±0.002
14	90	7500	20	196.84±0.003
15	30	7500	80	216.00±0.001
16	60	10000	20	195.87±0.000
17	60	5000	20	165.46±0.000

*Data are given as the mean (n=3)±standard deviation

Table 5 demonstrates the statistical analysis indicators formed by the software according to the ANOVA test (at 95% of confidence interval). Probability (P)>F has been found lower than 0.05, which demonstrates that the model implies the statistical significance of the derived model [13]. The outcome of the ANOVA test displays that R^2 and R^2_{adj} are in agreement, which is an indicator of the sufficient correlation between the actual and estimated findings [14]. Besides, poor value (6.65%) for the coefficient of variance (C.V.) indicates the higher accuracy of the prediction. However, the

Table 4. Model equation with coded factors derived by BBN design through RSA

Response	Equation	R^2
OC (mg/L)	$236.39+36.64\ X_1+19.30\ X_2+34.68X_3+15.71X_1\ X_2+4.84X_1\ X_3+8.18X_2\ X_3-1.22X_1^2+4.62X_2^2-23.91X_3^2$	0.9447

Table 5. ANOVA test generated by Design-Expert software (version 11) for the HAE of olive leaves

Source	Sum of squares	Degree of freedom	Mean square	F-value	Probility (P)>F
Model	27163.64	9	3018.18	13.27	0.0013
X_1-Time	10737.72	1	10737.72	47.23	0.0002
X_2-Speed	2978.38	1	2978.38	13.10	0.0085
X_3-EtOH concentration	9622.31	1	9622.31	42.32	0.0003
$X_1\ X_2$	987.22	1	987.22	4.34	0.0757
$X_1\ X_3$	93.80	1	93.80	0.4126	0.5411
$X_2\ X_3$	267.32	1	267.32	1.18	0.3141
X_1^2	6.30	1	6.30	0.0277	0.8725
X_2^2	90.04	1	90.04	0.3960	0.5491
X_3^2	2406.76	1	2406.76	10.59	0.0140
Residual	1591.51	7	227.36		
Lack of fit	1573.24	3	524.41	114.79	0.0002
Pure error	18.27	4	4.57		
Cor total	28755.15	16			

value found for lack of fit was not non-significant (P<0.05). Similarly, Khajeh [15] reported a significant value (P<0.05) for the lack of fit, where BBN design applied through RSA for the determination of zinc through microwave-assisted extraction [15]. Wang et al. also declared a significant lack of fit value by BBN design of RSA for ultrasound-assisted extraction of ρ-hydroxybenzaldehyde from *Sparganii rhizome* [16]. Kittisuban et al. declared that lack of fit with a significant value might be acceptable if there are numerous data in the relevant process system [17].

As seen in Table 5, extraction time was found to be the most effective process parameter for the relevant HAE system with the highest F value (10737.72). Time effect was also found to be statistically the most significant parameter in extraction of anthocyanins from red raspberries of Chen et al. [18]. Mokhtar et al. also found the time as the most prominent variable for the extraction of a model diesel with *N*,*N*-dimethylformamide according to the findings of BBN design [19]. In the same way, Liu et al. reported extraction time as the most important independent parameter depending on the findings of RSA for the supercritical fluid extraction of *Passiflora* seed oil [20]. This output was followed by solvent concentration, speed and the second-term of speed (at P<0.05).

3. Optimization of HAE

Three-dimensional (3D) plots generated by the proposed model (Table 3) are given in Figs. 3(a), (b) and (c). Fig. 3(a) demonstrates the effects of EtOH concentration and extraction time on OC in olive leaf extract. Increasing the concentration of the EtOH in the solvent solution gave rise to higher yield of OC. This outcome is consistent with that of Wang et al. [21], where they extracted biophenols from wheat bran by ultrasound. They reported total polyphenols rose slowly by EtOH quantity in the aqueous solution, and nearly attained a peak at the greatest concentration in their range tested. Regarding extraction time, there was a markable increase (a). Zhong and Wang [22], Silva et al. [23] and Ramić et al. [24] also had similar monitoring for time effect on the extraction of various natural products. Fig. 3(b) indicates that mixing speed had a slight effect on olive leaf extract rich in OC. The clear influence of speed and EtOH concentrations on the OC yield under a certain extraction time is also observed in Fig. 3(c).

4. Validation Study

Table 6 presents the optimum extraction conditions for the olive leaf extract obtained by HAE. The calculated finding along with optimal conditions according to the RSA by Design-Expert software is given in Table 6. To confirm the adequacy of the second-

Table 6. Comparison of the experimental and calculated results of the maximum OC by HAE

Optimum HAE conditions		Minimum OC (mg/L)		Error (%)
		Experimental	Predicted	
X_1 (s)	87.01			
X_2 (rpm)	9977.19	325.96	330.41	1.37
X_3 (%, v/v)	68.38			

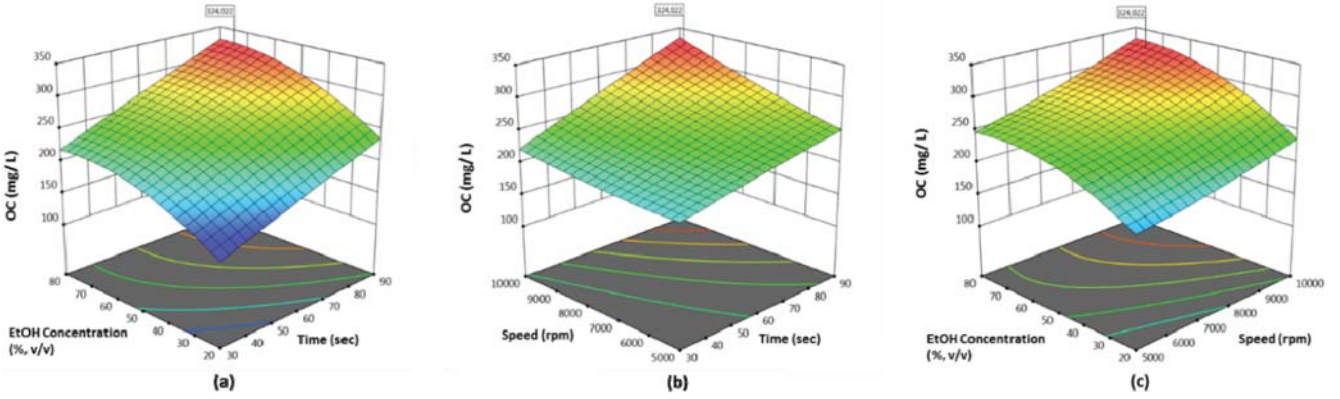

Fig. 3. 3D plots (a) as a function of solvent concentration to extraction time (speed=9,695.05 rpm), (b) as a function of speed to extraction time (EtOH concentration=72.39), (c) as a function of solvent concentration to speed (time=87.89 s).

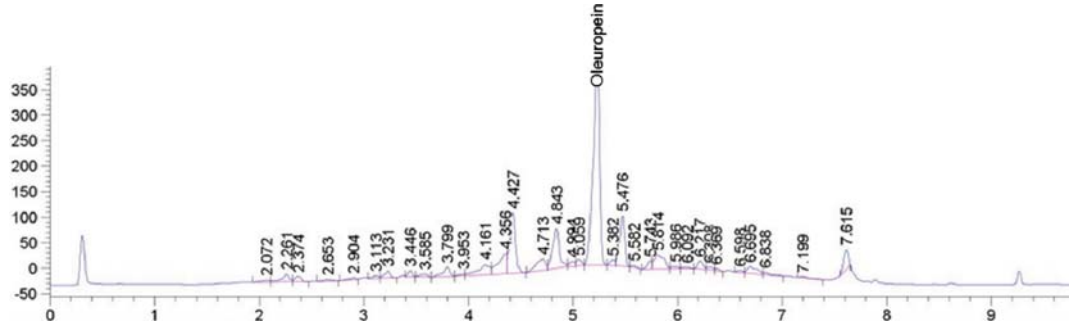

Fig. 4. HPLC chromatogram of olive leaf extract.

Table 7. Antioxidant properties of the olive leaf extract obtained by HAE

TBC (mg-GAE/g-DW)	DPPH (mg-TAEC/g-DW)	CUPRAC (mg-TAEC/g-DW)	TFC (mg-TAEC/g-DW)
44.79±0.005	94.91±0.002	177.68±0.001	34.74±0.003

*Data are given as the mean (n=3)±standard deviation

order polynomial model calculated by the software, an experimental study under the proposed optimum conditions was also conducted. Extremely poor residual (1.26%) between the actual and estimated values proved the fitness of the second-order polynomial model for estimation of the best response.

5. Evaluation of the Antioxidant Properties of Olive Leaf Extract

As seen in Fig. 4, olueropein is the leading biophenol of the olive leaf extract. Table 7 demonstrates the quantitative results of the spectrophotometric analysis of the olive leaf extract obtained by HAE under optimum conditions (87 sec of extraction with 68% EtOH solution at 9,977 rpm of homogenizer speed). The results of bioactive properties were given by several (gallic acid-GAE, catechin-CE and trolox-TAEC) equivalences per g of dried weight (mg/g-DW). Our findings are in agreement with those of the previous studies on the bioactive ingredients of olive leaf extract. Bilgin and Şahin [25] reported a total phenols yield ranging from 10.11 to 61.66 mg-GAE/g-DW through HAE depending on the geographical origin [25]. Elhussein and Şahin [26] also found similar content (40.97-48.07 mg-GAE/g-DW) of total biophenols by ultrasound-assisted extraction through 50% (v/v) methanol solution [26]. Regarding TFC, similar quantity was also observed as 31.99 mg-CE/g DW, where olive leaves were extracted by ultrasound-assisted extraction with 43.61% (v/v) EtOH solution [27]. Likewise, Şahin et al. declared that olive leaf extract obtained by HAE had TFC between 32.34 and 36.34 mg-CE/g-DW [28]. However, their antioxidant activity (DPPH) results (26.40-26.52 mg-TAEC/g-DW) were lower than that of the present study. This might be explained by many factors, such as the solvent system used, origin and cultivar of the plant and harvesting time.

6. Electrochemical Behavior of Oleuropein on Ti-rGO Modified GCE

Fig. 5 shows the molecular structure of the oleuropein in 3D (left side) and 2D views (right side) obtained by Avogadro molecular modeling software program with Open Babel version of 2.3.2.

SWV technique was performed to compare the electrochemical performance of 0.1 M oleuropein on both of the electrodes (Fig. 6). From the figure, a more sensitive and well-shaped oxidation curve is observed when the Ti-rGO modified electrode is used for the detection of oleuropein. The current density of oleuropein on Ti-rGO@GCE is calculated as 79 μMcm^{-2} while that of the GCE is lower than 10 μMcm^{-2}. The observed significant enhancement on the voltammogram is attributed to the high surface area of Ti-rGO nanocomposite, which enables oleuropein molecules to bind easily to the surface. On the other hand, the electron and the charge transfer abilities between the rGO layers and the oleuropein make the contribution to the enhancement of the peak responses due to the unique electrical properties of reduced graphene [55,56]. Integration of TiO_2 with rGO is expected to increase van der Waals

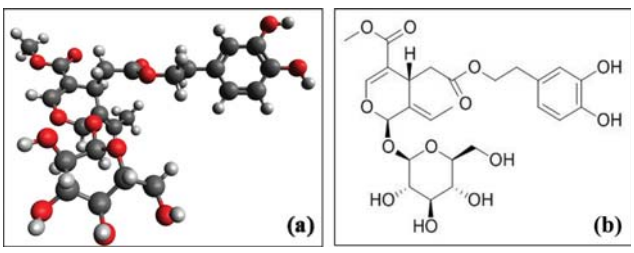

Fig. 5. Molecular structure of the oleuropein in 3D (a) and 2D views (b).

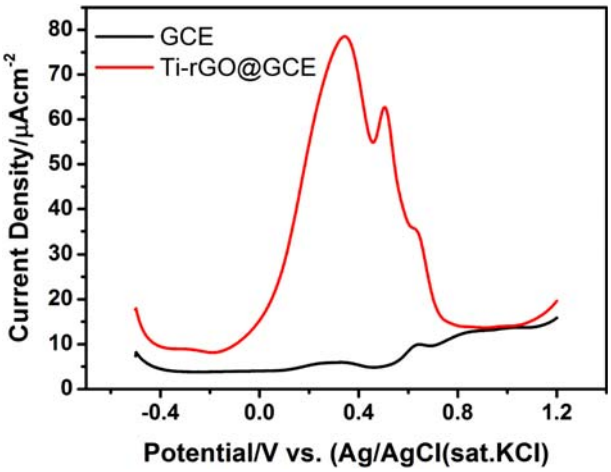

Fig. 6. Comparison of SWVs of 10 mM of olueropein on GCE and Ti-rGO@GCE in 0.1 M H_2SO_4 solution (The step size of 2 mV, frequency of 50 Hz and pulse size of 0.1 V are applied).

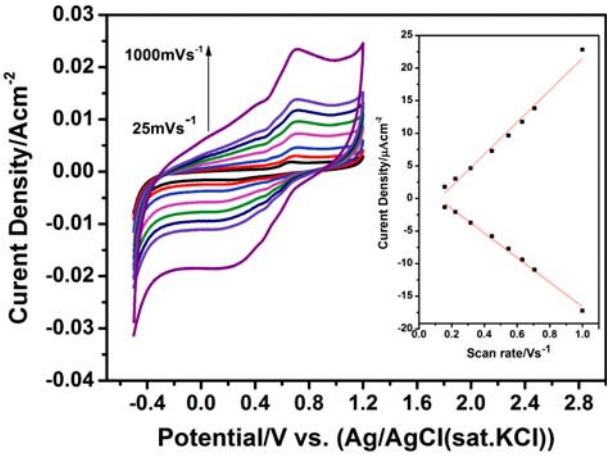

Fig. 7. CVs of 0.1 mM oleuropein on Ti-rGO@GCE at different scan rates from 25 to 1,000 mV s^{-1} in 0.1 M H_2SO_4. Inset shows the variation of square roots of scan rates versus current densities.

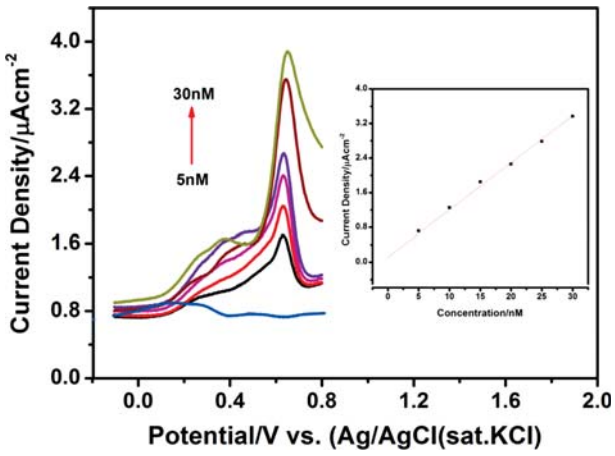

Fig. 8. Anodic SWVs for different concentrations of oleuropein on the Ti-rGO@GCE in the 0.1 M H_2SO_4 solution (pulse size 100 mV, frequency 50 Hz), inset: calibration curves prepared from SW voltammograms.

interactions between the Ti-O surface and the rGO domains, which enhance the electron transfer kinetics [57].

Fig. 7 shows the influence of the scan rate on current densities of 0.1 mM oleuropein on Ti-rGO@GCE. Different scan rates ranging from 25 to 1,000 mVs^{-1} are performed to analyze the reaction mechanism. From the peak separations of anodic and cathodic peaks of CV curves, it is revealed that a quasi-reversible process dominated the reaction mechanism. As a function of increasing scan rate, peak currents increase linearly while the peak potentials do not alter for the anodic part of the CV curves. A linear fit was observed when the peak current densities were plotted against the square root of the scan rates, suggesting the diffusion controlled and homogeneous reaction mechanism dominates the electrochemical behavior of this system (Fig. 7 inset).

SWV was applied for the quantitative determination of oleuropein using Ti-rGO@GCE. As shown in Fig. 8, prominent oxidation peaks were obtained at about 0.52 V on Ti-rGO@GCE. A plot of the anodic peak current densities of the oleuropein versus concentration (in nM) was found to be linear, and the limit of detection (LOD=3σ/slope) was calculated as $6.5\pm0.08\times10^{-10}$ M, utilizing the linearity range of 5-30 nM shown in the inset of Fig. 8. The limit of quantification (LOQ=10σ/slope) was calculated as $6.5\pm0.08\times10^{-10}$ M (The σ represents the standard deviation of nine samples shown in the figure). We used square wave voltammetry (SWV) technique because it is a very sensitive technique that enables direct analysis at the ppb (parts per billion) level and approximately 100-times faster analysis than other electro analytical techniques such as differential pulse, linear sweep, and cyclic voltammetry. It is a useful method to understand mechanisms of much faster chemical reactions. Furthermore, it is possible to study in multi component systems. The results provide improved resolution for a specific target molecule or analyte.

Taken together, these results suggest that the Ti-rGO@GCE is a highly sensitive electrode for quantitative determination of the trace amount of oleuropein. The high sensitivity of Ti-rGO@GCE towards oleuropein determination is attributed to the porous structure and the excellent conductivity of Ti-rGO nanocomposite. Compared with the previously published studies, the present study shows significant improvement in the sensitive determination of oleuropein on carbon based electrodes using electrochemical techniques [30-32].

CONCLUSION

A new TiOx modified rGO based nanocomposite has been developed to determine the trace amount of oleuropein which was extracted from olive leaves using HAE method. The morphological and structural characterization of the fabricated electrode showed high surface area due to the porous nature of Ti-rGO nanocomposite. A quasi-reversible process influenced the reaction mechanism. SWV results showed the LOD value of 0.57 nM with the correlation coefficient of 0.9988 in the linear concentration range of 05-30 nM.

CONFLICT OF INTEREST

The authors declare that there is no conflict of interest in writing upon submission of the manuscript.

REFERENCES

1. N. Mirabella, V. Castellani and S. Sala, *J. Clean. Prod.*, **65**, 28 (2014).
2. A. P. Pereira, I. C. Ferreira, F. Marcelino, P. Valentão, P. B. Andrade, R. Seabra, L. Estevinho, A. Bento and J. A. Pereira, *Molecules*, **12**(5), 1153 (2007).
3. S. Şahin and M. Bilgin, *J. Sci. Food Agric.*, **98**(4), 1271 (2017).
4. S. Souilem, I. Fki, I. Kobayashi, N. Khalid, M. A. Neves, H. Isoda, S. Sayadi and M. Nakajima, *Food Bioprocess Technol.*, **10**(2), 229 (2017).
5. M. Mohamadi, A. Mostafavi and M. Torkzadeh-Mahani, *Bioelectrochemistry*, **101**, 52 (2015).
6. M. Cittan, S. Koçak, A. Çelik and K. Dost, *Talanta*, **159**, 148 (2016).
7. Y. A. Aydın and N. D. Aksoy, *Chem. Eng. J.*, **151**(1-3), 188 (2009).
8. N. S. A. Malik and J. M. Bradford, *Sci. Hortic. (Amsterdam)*, **110**(3), 274 (2006).
9. S. Sakanaka, Y. Tachibana and Y. Okada, *Food Chem.*, **89**(4), 569 (2005).
10. J. Yu, L. Wang, R. L. Walzem, E. G. Miller, L. M. Pike and B. S. Patil, *J, Agric. Food Chem.*, **53**(6), 2009 (2005).
11. S. Şahin and R. Şamlı, *Ultrason. Sonochem.*, **20**(1), 595 (2013).
12. R. Apak, K. Güçlü, M. Özyürek and S. E. Çelik, *Microchim. Acta*, **160**(4), 413 (2008).
13. B. K. Körbahti and A. Tanyolaç, *J. Hazard. Mater.*, **151**(2-3), 422 (2008).
14. Jagadish, S. Bhowmik and A. Ray, *Int. J. Adv. Manuf. Technol.*, **87**(5-8), 1359 (2016).
15. M. J. Khajeh, *Food Compos. Anal.*, **22**(4), 343 (2009).
16. X. Wang, Y. Wu, G. Chen, W. Yue, Q. Liang and Q. Wu, *Ultrason. Sonochem.*, **20**(3), 846 (2013).
17. P. Kittisuban, P. Ritthiruangdej and M. Suphantharika, *LWT - Food Sci. Technol.*, **57**(2), 738 (2014).
18. F. Chen, Y. Sun, G. Zhao, X. Liao, X. Hu, J. Wu and Z. Wang, *Ultrason. Sonochem.*, **14**(6), 767 (2007).

19. W. N. A. W. Mokhtar, W. A. W. A. Bakar, R. Ali and A. A. A. Kadir, *J. Taiwan Inst. Chem. Eng.*, **45**(4), 1542 (2014).
20. S. Liu, F. Yang, C. Zhang, H. Ji and P. Hong, *J. Supercrit. Fluids*, **48**(1), 9 (2009).
21. J. Wang, B. Sun, Y. Cao, Y. Tian and X. Li, *Food Chem.*, **106**(2), 804 (2008).
22. K. Zhong and Q. Wang, *Carbohydr. Polym.*, **80**(1), 19 (2010).
23. E. M. Silva, H. Rogez and Y. Larondelle, *Sep. Purif. Technol.*, **55**(3), 381 (2007).
24. M. Ramić, S. Vidović, Z. Zeković, J. Vladić, A. Cvejin and B. Pavlić, *Ultrason. Sonochem.*, **23**, 360 (2015).
25. M. Bilgin and S. Şahin, *J. Taiwan Inst. Chem. Eng.*, **44** (1), 8 (2013).
26. E. A. A. Elhussein and S. Şahin, *Heat Mass Transf.*, **54**, 1901 (2018).
27. S. Şahin, Z. İlbay and S. İ. Kırbaşlar, *Sep. Sci. Technol.*, **50**(8), 1181 (2015).
28. S. Şahin, E. Elhussein, M. Bilgin, J. M. Lorenzo, F. J. Barba and S. Roohinejad, *J. Food Process. Preserv.*, **42**(5), 1 (2018).
29. J. Wang, Electroanalytical Techniques in Clinical Chemistry and Laboratory Medicine, VCH Publishers (1988).
30. M. Mohamadi, A. Mostafavi and M. Torkzadeh-Mahani, *Bioelectrochemistry*, **101**, 52 (2015).
31. M. Cittan, S. Kocak, A. Celik and K. Dost, *Talanta*, **159**, 148 (2016).
32. F. J. V. Gomez, A. Spisso and M. Fernanda Silva, *Electrophoresis*, **38**(21), 2704 (2017).
33. G. H. Lee, R. C. Cooper, S. J. An, S. Lee, A. van der Zande, N. Petrone, A. G. Hammerberg, C. Lee, B. Crawford, W. Oliver, J. W. Kysar and J. Hone, *Science*, **340**(6136), 1073 (2013).
34. H. Bagheri, A. Hajian, M. Rezaei and A. Shirzadmehr, *J. Hazard. Mater.*, **324**, 762 (2017).
35. P. Bollella, G. Fusco, C. Tortolini, G. Sanzò, G. Favero, L. Gorton and R. Antiochia, *Biosens. Bioelectron.*, **89**, Part 1, 152 (2017).
36. D. A. C. Brownson, D. K. Kampouris and C. E. Banks, *J. Power Sources*, **196**(11), 4873 (2011).
37. G. Eda and M. Chhowalla, *Adv. Mater.*, **22**(22), 2392 (2010).
38. C. I. L. Justino, A. R. Gomes, A. C. Freitas, A. C. Duarte and T. A. P. Rocha-Santos, *TrAC Trends Anal. Chem.*, **91**, 1 (2017).
39. F. Li, X. Jiang, J. Zhao and S. Zhang, *Nano Energy*, **16**, 488 (2015).
40. A. Gutés, C. Carraro and R. Maboudian, *Biosens Bioelectron.*, **33**(1), 56 (2012).
41. H. Yu, B. Zhang, C. Bulin, R. Li and R. Xing , *Scientific Reports*, **6**, 36143 (2016).
42. B. Mendoza-Sánchez, J. Coelho, A. Pokle and V. Nicolosi, *Electrochim. Acta*, **174**, 696 (2015).
43. S. Pei and H.-M. Cheng, *Carbon*, **50**(9), 3210 (2012).
44. K. Kakaei and K. Hasanpour, *J. Mater. Chem. A.*, **2**(37), 15428 (2014).
45. D. R. Dreyer, S. Park, C. W. Bielawski and R. S. Ruoff, *Chem. Soc. Rev.*, **39**(1), 228 (2010).
46. G. Venugopal, K. Krishnamoorthy, R. Mohan and S.-J. Kim, *Mater. Chem. Phys.*, **132**(1), 29 (2012).
47. S. Şahin and M. Bilgin, *Sep. Sci. Technol.*, **47**(16), 2391 (2012).
48. E. Andrijanto, S. Shoelarta, G. Subiyanto and S. Rifki, *Aip Conf. Proc.*, **1725**(1), 020003 (2016).
49. J. R. Ferraro and A. J. Rein, Eds. Academic Press, Inc.: Orlando, Florida, **4** (1985).
50. R. A. Yadav, P. Rani, M. Kumar, R. Singh, P. Singh and N. P. Singh, *Spectrochim. Acta Part A: Mol. Biomol. Spectrosc.*, **84** (1), 6 (2011).
51. Sudesh, N. Kumar, S. Das, C. Bernhard and G. D. Varma, *Supercond. Sci. Technol.*, **26**(9), 1 (2013).
52. C. Zhang, D. M. Dabbs, L.-M. Liu, I. A. Aksay, R. Car and A. Selloni, *J. Phys. Chem. C.*, **119**(32), 18167 (2015).
53. P. Benjwal, M. Kumar, P. Chamoli and K. K. Kar, *RSC Adv.*, **5**(89), 73249 (2015).
54. N. Hu, Z. Yang, Y. Wang, L. Zhang, Y. Wang, X. Huang, H. Wei, L. Wei and Y. Zhang, *Nanotechnology*, **25**(2), 025502 (2014).
55. P. Suvarnaphaet and S. Pechprasarn, *Sensors (Basel, Switzerland)*, **17**(10), 2161 (2017).
56. P. R. Solanki, S. Srivastava, M. A. Ali, R. K. Srivastava, A. Srivastava and B. D. Malhotra, *RSC Adv.*, **4**(104), 60386 (2014).
57. J.-H. Yun, R. J. Wong, Y. H. Ng, A. Du and R. Amal, *RSC Adv.*, **2**(21), 8164 (2012).
58. B. Paulchamy, G. Arthi and B. D. Lignesh, *Nanomaterial. J. Nanomed Nanotechnol.*, **6**, 253 (2015).